



Structural, morphological, dielectric and impedance spectroscopy of lead-free $\text{Bi}(\text{Zn}_{2/3}\text{Ta}_{1/3})\text{O}_3$ electronic material

S. Halder¹ · S. Bhuyan¹ · S. N. Das¹ · S. Sahoo¹ · R. N. P. Choudhary¹ · P. Das² · K. Parida¹

Received: 3 June 2017 / Accepted: 12 November 2017 / Published online: 17 November 2017
© Springer-Verlag GmbH Germany, part of Springer Nature 2017

Abstract

A lead-free dielectric material $[\text{Bi}(\text{Zn}_{2/3}\text{Ta}_{1/3})\text{O}_3]$ has been prepared using a solid state reaction technique at high-temperature. The resistive, conducting and capacitive characteristics of the prepared electronic material have been studied in different experimental conditions. The determination of basic crystal parameters and reflection indices confirm the development of polycrystalline compound with orthorhombic crystal structure. The study of frequency–temperature dependence of ac conductivity illustrates the nature and conduction mechanism of the material. On the basis of observed impedance data and detailed dielectric analysis, the existence of non-Debye type relaxation has been affirmed. The electronic charge carriers of compound have short range order that has been validated from the complex modulus and impedance spectrum. The detailed studies of resistive, capacitive, microstructural characteristics of the prepared material provide some useful data for considering the material as an electronic component for fabrication of devices.

1 Introduction

During the present worldwide rebellion in electronic ceramic manufacturing unit, the fabrication of resonators and ceramics based devices has been one of the rapidly growing areas. Recently, researcher and scientists are much attracted towards development of complex perovskite materials for their promising applications for large as well as miniaturizing passive microwave components, capacitors, filters, resonators, etc. Nowadays, there is an enormous demand to fabricate ideal ceramic components with some distinct properties, such as, high value of dielectric constant, thermally stable resonant frequency and effectively low tangent loss [1–6]. With the advancement of the technology in the mobile communication, sensor, transducer, memory devices, low-temperature fired high-density ceramics, etc., have been in a great demand [7]. Most of the high performance dielectrics, which have high sintering temperature, become unsuitable for device applications [8]. Based on certain assorted and attractive physical properties, such as,

piezoelectric, superconductivity, ferroelectric, ionic conductivity, etc., some dielectric materials with perovskite structure have been considered as important materials for various electronic devices. For this purpose, materials of different structural families have also been used. Out of all, compounds of perovskite structural family have been found most suitable and useful. The member of perovskite structural family (having a general formula ABO_3) can be pulled out to a larger scope by incorporating two or more cations at the ‘B’ site (i.e., $\text{AB}'_{1-x}\text{B}''_x\text{O}_3$). Based on the ionic size and amount of two or more substituted elements at the A/B sites, the number of perovskite compounds can be increased further [9–12]. Among all the pure or complex perovskites, lead zirconate titanate and its polymer-based materials have been found very useful for various devices [13, 14]. Because of the toxic nature of lead/lead-based compounds, efforts are now being made to develop eco-friendly (lead-free) compounds for different devices. Though various attempts have been made in this direction, some bismuth-based dielectric materials have drawn much attention of the researchers because of their excellent physical properties and cost effective fabrication. To fabricate lead-free perovskite ceramic, bismuth oxide (Bi_2O_3) has been identified as a good ingredient with some inherent problems, such as high ionic conductivity, structural instability, evaporation during high-temperature processing, etc. To reduce or eliminate these problems, several oxides have been combined to

✉ S. Bhuyan
satyanarayanbhuyan@soauniversity.ac.in

¹ Siksha ‘O’ Anusandhan University, Bhubaneswar 751030, India

² Department of Physics, Midnapore College, Midnapore, West Bengal 721101, India

Bi_2O_3 [15]. Combining niobium pentoxide (Nb_2O_5) and zinc oxide (ZnO) to bismuth oxide in a stoichiometric ratios, we get a stable compound (bismuth zinc niobate) with interesting physical properties, including high dielectric constant, low tangent loss, low sintering temperature, reduced cost of electrode materials, etc., [16, 17]. Thus, bismuth-based (lead-free) compounds (perovskite or distorted perovskite) can be derived for devices because of their inherent flexibility that can be attained by chemical manipulation and/or by choosing suitable fabrication techniques. To outline the elemental features or various characteristics (including dielectric and impedance spectroscopy) of $\text{Bi}(\text{Zn}_{2/3}\text{Ta}_{1/3})\text{O}_3$ (BZT), processed using a mixed oxide technique, have been studied. In this communication, structural, dielectric and electrical properties of this environmental friendly bismuth zinc tantalum have been reported.

2 Experimental

$\text{Bi}(\text{Zn}_{2/3}\text{Ta}_{1/3})\text{O}_3$ is synthesized using high-purity (> 99.5%) analytical grade ingredients (oxide powders); Bi_2O_3 , ZnO , and Ta_2O_5 (M/S Loba Chemical, India) by a method based on reaction of solid oxides at higher-temperatures. To fabricate BZT, fine powder of the above oxides is first weighted carefully in desired stoichiometry, and then mixed thoroughly using agate mortar via dry and wet grinding. The homogeneous mixture of the oxides is fired in four steps up to 800 °C, and then calcined in a controlled atmosphere for 8 h in covered alumina crucible. X-rays diffraction data and reflection profiles of the calcined powder of $\text{Bi}(\text{Zn}_{2/3}\text{Ta}_{1/3})\text{O}_3$ are collected in a wide range of diffraction angle ($20^\circ\text{C} \leq 2\theta \leq 70^\circ\text{C}$) with $\text{CuK}\alpha$ radiation and scanning rate of $2^\circ/\text{min}$ to reveal the formation of the compound (BZT). An organic binder poly-vinyl alcohol (PVA) used to make disk type pellets from fine calcinated powders using a hydraulic press. Finally, disc shape samples are sintered for a period of 12 h at 770 °C in high-temperature furnace. Then, a compacted pellet sample is electroded by firing them with silver paste to measure the frequency and temperature dependent electrical properties. The structural parameters of the material are calculated using 'POWD' software package by indexing all the peaks of the oxide powder. SEM (scanning electron microscopy) along with EDX (energy dispersive analysis of X-rays) and mapping image of elements have been used to examine the changes in microstructure and chemical composition of the fabricated pellet. The impedance/LCR meter (computer-controlled) has been utilized to measure the electrical and dielectric parameters of the fabricated compound at selected range of frequency (10^3 – 10^6 Hz) and temperature 100–500 °C.

3 Experimental results and analysis

Figure 1 illustrates X-ray diffraction spectrum of calcinated $\text{Bi}(\text{Zn}_{2/3}\text{Ta}_{1/3})\text{O}_3$ at room temperature. As the location and intensity of all the distinct reflection peaks differ from those of ingredients [18], the formation of single phase polycrystalline compound of BZT is assumed. To obtain crystal data and basic crystal structure of the compound, the intensity peaks are indexed in all seven crystal system through software, POWD [19]. With the help of best fit (i.e., the smallest difference between the experimental and proposed model value of inter-planar spacing and diffraction angle of each reflection), orthorhombic crystal system is selected. The refined lattice parameters are obtained using least-squares refinement routine: $a = 3.5723 \text{ \AA}$, $b = 36.8150 \text{ \AA}$ and $c = 13.4670 \text{ \AA}$. The normalized unit cell dimension of the orthorhombic cell can be written as; $a' = 3.5723 \text{ \AA}$, $b' = b/10 = 3.6815 \text{ \AA}$ and $c' = 13.467/2 \times 3^{1/2} = 3.8877 \text{ \AA}$. These unit cell dimension is very much consistent with those of distorted perovskite in orthorhombic phase. The distorted perovskite of the compound can also be explained on the basis of tolerance factor as follow. The perovskite structure of the compound can be signified from charge balance and tolerance factor (t). The t is known by Goldschmidt tolerance factor. This factor gives an indication of the stability as well as distortion of the crystal structure, and is defined as $t = \frac{r_A + r_o}{\sqrt{2}(r_B + r_o)}$, where r_A and r_B are ionic radius of A and B site atoms and r_o is the ionic radius of O^{2-} . The tolerance factor of ideal perovskite is $t = 1$. While using the above formula, the tolerance factor of the present studied compound is found to be 0.82 which is less than ideal perovskite. Therefore, this compound shows distorted perovskite structure. The

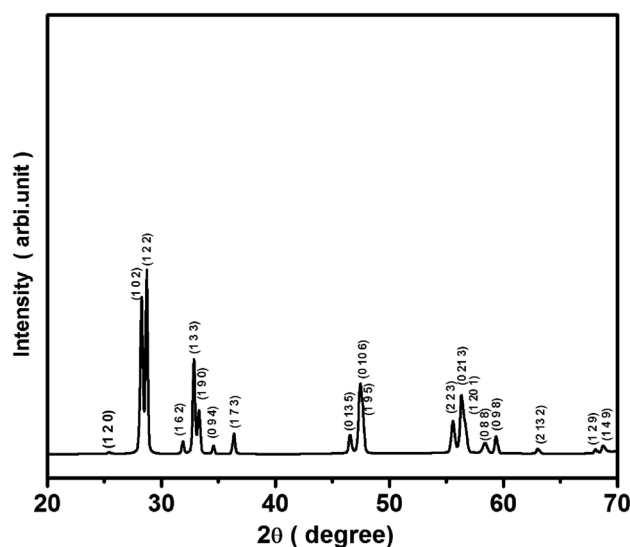


Fig. 1 XRD pattern of $\text{Bi}(\text{Zn}_{2/3}\text{Ta}_{1/3})\text{O}_3$

tolerance factor for orthorhombic phase of perovskite lies between 0.71 and 0.9 [20]. As the calculated tolerance factor of the synthesized material (0.82) lies between the above limit, it supports the conclusion drawn about the selected of orthorhombic system of the fabricated compound. If the value of t is closer to 1, then the structure can be regarded as stable. Based on the value of t , it can be concluded that the synthesized compound is relatively less stable perovskite. The crystallite size of the sample, calculated using the Scherrer's formula; $P_{hkl} = k\lambda/\beta_{1/2} \cos \theta$ with wavelength $\lambda = 1.5405 \text{ \AA}$ and k (constant) = 0.89, $\beta_{1/2}$ = broadening of the peak (full width half maxima), is found to be 38 nm.

The surface morphology of BZT can be revealed from the scanning electron microscopic image of sintered pellets as shown in Fig. 2. Grains of different dimensions and shapes have been distributed homogeneously over the surface that can be noticed from the micrograph. The high density of the sample also can be suggested. The high-temperature sintering of the sample has helped to get almost free from irregular shape of voids. From the microscopic images analysis it can be concluded that the grain growth or agglomeration of smaller grains is dependent on processing temperature [21]. The EDX (energy dispersive X-ray spectroscopy analysis) displays the elemental components and composition of the high-temperature sintered pellet (BZT). The EDX spectra of the compound show the presence of bismuth, zinc, tantalum in required amount of BZT sample (Fig. 2). Thus, nature and presence of elements in the EDX spectra support the formation of single phase compound. It also confirms the purity of the sample due to the nonexistence of extra elements [other than (Bi, Zn, Ta)] in the compound. As there is a very small difference in the calculated and observed (experimental) weight percent (Wt%) of heavy atoms Bi (0.83%), Zn (1.5%) and Ta (2.7%), the formation of single phase compound with said stoichiometry

is confirmed. However, because of low atomic weight of oxygen, error in Wt% is found little higher (7.7%). The elemental mapping and distributions of different elements (Bi, Zn, Ta, O) of the sample surface (shown in Fig. 2) have further support on the development of the required compound.

At the present time, complex impedance spectroscopy (CIS) scheme is widely adopted to examine structure–properties relation of polycrystalline ionic and ferroelectric materials. It is an influential flexible tool for creating the association between dielectric and electrical characteristics as well as to find out the consequence of grains including grain boundaries as well as interface in the synthesized compound.

Figure 3 represents the temperature reliance of relative dielectric constant (ϵ_r) and tangent loss ($\tan \delta$) of the compound $\text{Bi}(\text{Zn}_{2/3}\text{Ta}_{1/3})\text{O}_3$ at certain frequencies like 1, 10, 100, 500, and 1 MHz. Both the parameters [dielectric constant (ϵ_r) and tangent loss ($\tan \delta$)] descend on rising frequency which is a usual tendency of the dielectric compound. For

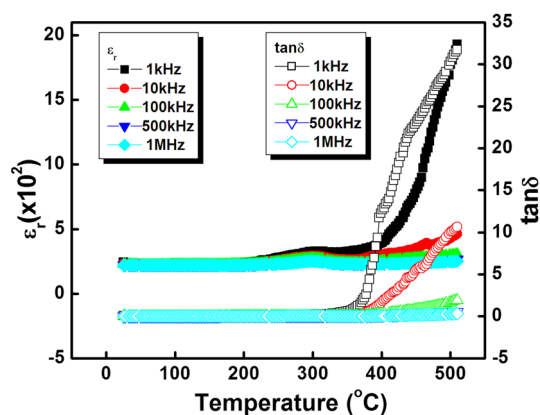


Fig. 3 Temperature dependence of dielectric constant and tangent loss at selected frequencies of $\text{Bi}(\text{Zn}_{2/3}\text{Ta}_{1/3})\text{O}_3$

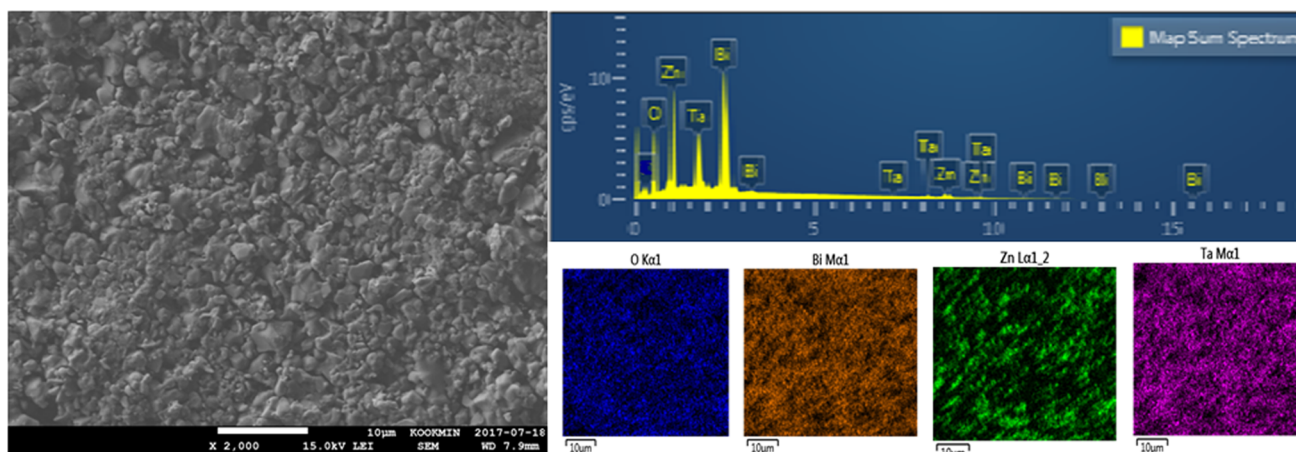


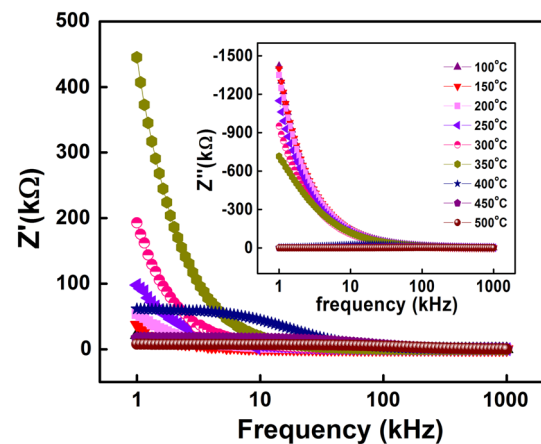
Fig. 2 SEM, EDX spectra and distribution of different element of $\text{Bi}(\text{Zn}_{2/3}\text{Ta}_{1/3})\text{O}_3$

Table 1 Elemental weight percentage of the compound $\text{Bi}(\text{Zn}_{2/3}\text{Ta}_{1/3})\text{O}_3$

Element	(Observed)Wt%	(Calculated)Wt%	Error (%)
O	14.32	13.29	7.7
Zn	11.77	12	2.7
Ta	16.46	16.71	1.5
Bi	57.42	57.90	0.83

low-frequency region, the specimen compound has high dielectric constant that resulted may be because of space charge polarization caused by accumulation of free electrons. From the plot, it can be identified that the $\tan \delta$ rises sharply in the region of low-frequency while its value declines swiftly at higher-temperatures with increase in frequency. However, for BZT compound, no phase transition has been observed in extensive operating frequency and temperature (100–500 °C) [22]. It is observed that the rise of tangent loss is quite slower in low-temperature region, but it increases significantly at high-temperature regions that may be due to absence of defects or vacancy in material and low thermally energized charge carriers. The dielectric and related parameters of fabricated material $\text{Bi}(\text{Zn}_{2/3}\text{Ta}_{1/3})\text{O}_3$ have been compared with those of similar compound, namely $\text{Bi}(\text{Zn}_{2/3}\text{Nb}_{1/3})\text{O}_3$ (Table 1), and found significant difference in them. For example, the value of tangent loss of $\text{Bi}(\text{Zn}_{2/3}\text{Nb}_{1/3})\text{O}_3$ is found much smaller ($\tan \delta = 5.10$) as compared to that of $\text{Bi}(\text{Zn}_{2/3}\text{Ta}_{1/3})\text{O}_3$ (i.e., $\tan \delta = 23.53$) at the same temperature (450 °C) and frequency (1 kHz) which is consistent with many compounds of such family. It can be observed that the trend of variation of dielectric constant (ϵ_r) with frequency and temperature is similar to that of loss tangent. Initially, the rise in dielectric constant is observed to be independent of temperature (i.e., up to 250 °C) that is due to the presence of different types of polarizations in the material in the low-frequency region. This effect of polarization disappears slowly on increasing frequency, and thus dielectric constant decreases. The value of ϵ_r was found to increase gradually on rising temperature till it reaches its maximum value (ϵ_{max}) at all selected frequency of BZT. Sometimes, the volatile nature of Bi and creation of oxygen vacancies during high-temperature processing of the sample [23] are also considered for the high value of dielectric constant. The relative dielectric constant of $\text{Bi}(\text{Zn}_{2/3}\text{Nb}_{1/3})\text{O}_3$ at 450 °C and frequency of 1 kHz is ($\epsilon_r = 3.6 \times 10^3$) while the dielectric constant of fabricated material $\text{Bi}(\text{Zn}_{2/3}\text{Ta}_{1/3})\text{O}_3$ is found to be ($\epsilon_r = 8.3 \times 10^2$) at same temperature and frequency.

Figure 4 illustrates the behaviour of real and imaginary part (Z' and Z'') of CIS with frequency at certain selected temperatures. It can be depicted that Z' declines continuously in the region of low-frequency with the increase in temperature which substantiate the negative temperature

**Fig. 4** Frequency variation of Z' and Z'' at different temperature of $\text{Bi}(\text{Zn}_{2/3}\text{Ta}_{1/3})\text{O}_3$

coefficient of resistance behaviour of this material. Irrespective of temperature, with the increase of frequency the real part of impedance spectrum curves merges in the high-frequency region to obtain an approximate constant value that may be due to the semi conduction properties and release of space charges at high-temperature [24]. The imaginary impedance component (Z'') versus frequency plots provide some new major characteristics, such as: (1) the spectrum peak point occurrence at a specific frequency, (2) at higher frequencies, merger of the impedance spectrum pattern and (3) the peak broadening with rise in temperature.

The Z'' increases with growth in temperature and frequency, and then by attaining maximum value (Z''_{max}), it then declines gradually which can be indicated from the loss spectrum. With the increase in temperature, the Z''_{max} shifts to the region of high-frequency suggesting a rise in tangent loss. The broadening and shifting of peaks occur due to decrement of bulk resistance with the temperature rise. It hints that thermally activated dielectric relaxation phenomenon takes place due to low-temperature static charges and vacancies at higher-temperatures. The occurrence of multiple relaxation times can also be signified from the asymmetric peak broadening.

The effect of large resistance and small capacitance can be investigated from frequency dependence of Z'' vs M'' (imaginary part of complex modulus) plot at a particular temperature of 400 °C (Fig. 5). The dissimilarity between the movement of short range and long range charge carriers in the relaxation process can also be identified from the given plot. The mismatch between Z''_{max} and M''_{max} peak at the same frequency and temperature will indicate the occurrence of the process due to movement of localized charge carrier while the presence of long-range type charge carriers can be signified from the complete merger of the two peaks at same frequency [25]. From the combined plot it can be

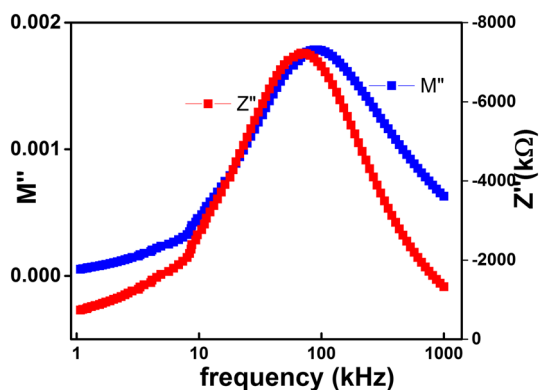


Fig. 5 Frequency variation of Z'' and M'' at 400 °C of Bi ($Zn_{2/3}Ta_{1/3}$) O_3

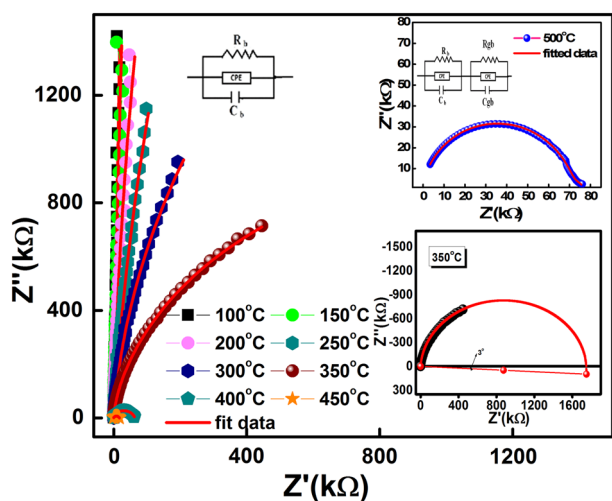


Fig. 6 Variation of Z' with Z'' as a function of temperature, and at 350 °C the depression angle of Bi($Zn_{2/3}Ta_{1/3}$) O_3

noticed that the peak of Z''_{max} slightly separated from M''_{max} which illustrate that the synthesized sample posses non-Debye relaxation with shorter mobility of charge carriers .

The Nyquist plot (Fig. 6) displays the frequency (1 kHz to 1 MHz) variation of impedance spectrum (Z' vs Z'') at some selected temperatures (100–500 °C). The impedance actions of the sample can be signified through the formation of semicircular arcs whose pattern of progression deviates with change in temperature. With the rise in temperature, the arc gradually bends towards the axis making semicircular arc even as its central point has shifted towards origin. With further temperature rise, the arc gradient decreases, and twirl towards real impedance axis which can be indicated from the Nyquist plot. The appearance of semicircular arc at a temperature above 450 °C indicate that electrical behaviour of the compound can be identified by estimating the contributions of grain interior (bulk material) and effects of grain-boundary. An equivalent electrical circuit model (Zsimpwin 2.0 version) made up of parallel connection between bulk resistance (R_b) and bulk capacitance (C_b) that is serially connected with parallel combination of grain-boundary resistance (R_{gb}), and thus grain-boundary capacitance (C_{gb}) has been used to study the relationship between theoretical and experimental data as illustrated in Fig. 6. Table 2 shows the extracted values of grain resistance (R_b), grain-boundary resistance (R_{gb}) bulk capacitance (C_b), and grain-boundary capacitance (C_{gb}) and bulk capacitance (C_{gb}) at various temperatures using the fitted curves. The symmetrical nature of semicircular arc (which centre lies at z-axis) suggests the Debye type of dielectric relaxation while depressed semi-circular arc (with centre below z-axis) occurs due to the in homogeneity and imperfection of the sample leads to distribution of relaxation time usually referred as non-Debye type of relaxation behaviour shows [26–28]. The graph confirms non-Debye type of behaviour that illustrates the depression angle of 3° and the centre below the z-axis at 350 °C.

The ac conductivity estimation has been done to realize the influence of temperature and frequency on the electrical properties of the material. Figure 7 illustrates the variation of ac conductivity as a function of frequency (1 kHz–1 MHz) at selected temperatures (100–500 °C). The σ_{ac} conductivity of the compound, calculated using measured dielectric

Table 2 Fitting parameters of Bulk and grain-boundary resistance as well as capacitance of impedance parameters of the compound Bi($Zn_{2/3}Ta_{1/3}$) O_3

Temperature (°C)	R_g (Ω)	C_g (F)	CPE	R_{gb} (Ω)	C_{gb} (F)	CPE _{gb}
100	8.692E+008	8.836E-012	1.132E-010	–	–	–
150	2.932E+008	4.686E-011	7.647E-011	–	–	–
200	4.602E+007	8.723E-011	1.306E-010	–	–	–
250	3.147E+007	8.723E-011	1.196E-010	–	–	–
300	6.212E+006	9.113E-023	2.175E-010	–	–	–
350	2.545E+006	1.107E-010	2.401E-009	–	–	–
400	6.373E+004	1.024E-010	2.049E-009	–	–	–
450	1.706E+004	1.045E-010	5.808E-009	–	–	–
500	4.399E+002	5.835E-011	7.232E-007	7.265E+003	9.236E-011	1.737E-009

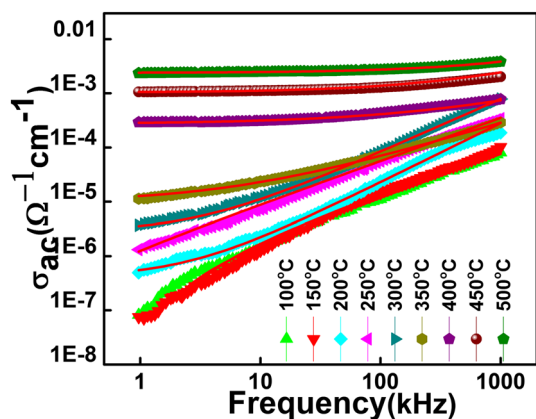


Fig. 7 Frequency dependent ac conductivity at selected temperature of $\text{Bi}(\text{Zn}_{2/3}\text{Ta}_{1/3})\text{O}_3$

parameters in equation; $\sigma_{ac} = \omega \epsilon \epsilon_0 \tan \delta$ (terms have their usual meanings), increases systematically with the rise in frequency (as observed from conductivity spectrum). This kind of trend in conductivity spectrum may be ascribed to the existence of space charges and dis-arranging of cations with rising frequency. However, on virtual investigating the conductivity spectra in the low-frequency region, plateau like region appears which is related to dc conductivity. In the high-frequency region, the frequency dependent curves tend to merge which is an indication of occurrence of dispersion phenomena. The conductivity dispersion of the fabricated material can be analyzed in a wide frequency range (dc to ac frequency) using the Jonscher's power law as [22]:

$$\sigma_{ac} = \sigma_{dc} + A\omega^n, \quad (1)$$

where A is temperature dependent constant and n is temperature dependent frequency exponent which lies between 0 and 1. It can be distinguished that with the increase in frequency conductivity rises while declining the build up charges that is a characteristic of ω^n . Frequency independent and flat response can be noticed at lower frequency and higher temperature. The deviation of conductivity can be recognized by the effect of polarization at the dielectric and electrode interface in the low-frequency region [22]. It is firmed that the factor A rises with temperature, whereas the factor n behaves in a reverse manner. With an impulsive hopping of charge carriers, a translational motion is entailed for $n < 1$, whilst for $n > 1$ a localized hopping is caused devoid of the species in the neighbourhood. Figure 8 shows the variation of A and n with temperature. It can be observed that the value of A is nearly constant upto 300 °C with the rise in temperature and after which it suddenly increases with increase in temperature. The A (pre-exponential factor) determines the strength of polarizability. As the value of A increases with rise in temperature it signifies the rise in polarizability and hence dielectric properties. The variation of dielectric

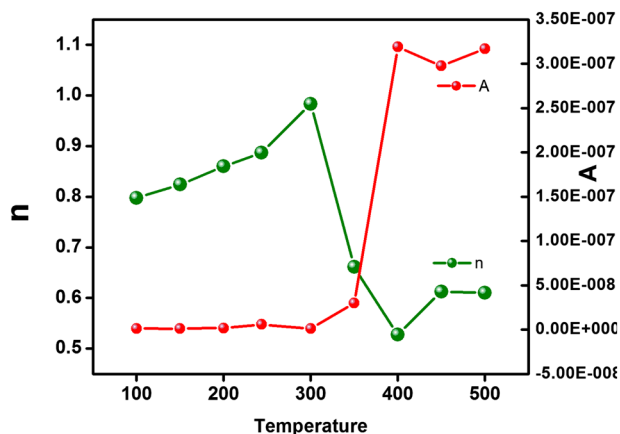


Fig. 8 n and A variation with temperature of $\text{Bi}(\text{Zn}_{2/3}\text{Ta}_{1/3})\text{O}_3$

properties as a function of temperature is similar to temperature dependent behaviour of pre-exponential factor. The exponent n has a reverse trend as its value declines with increase in temperature above (300 °C) and this decrement trend continues. The declining nature of n with temperature suggests that the strong interaction between the mobile ions and the lattice around them increases. At the same temperature of 450 °C and frequency of 1 kHz, $\text{Bi}(\text{Zn}_{2/3}\text{Nb}_{1/3})\text{O}_3$ and $\text{Bi}(\text{Zn}_{2/3}\text{Ta}_{1/3})\text{O}_3$ possess similar ac conductivity value ($\sigma_{ac} = 1 \times 10^{-3}$) [29].

Using the calculated ac conductivity (with dielectric parameters) and the following equation (2), the activation energy (E_a) at different temperature can be calculated.

$$\sigma_{ac} = \sigma_0 \exp(-E_a/kT), \quad (2)$$

where k = Boltzmann constant and σ_0 = pre-exponential conductivity. Based on the slope of the Arrhenius plot (Fig. 9), the depicted spectrum can be divided into different regions suggesting existence of multiple relaxation and conduction processes in the material [29]. It is found that with increasing temperature, ac conductivity of the sample increases which follows the thermally active transport mechanism in the compound. Using the above plot, the estimated value of activation energy is found to be 1.11, 1.0, 0.81, 0.59 and 0.57 eV for 1, 10, 100, 500 and 1000 kHz, respectively. Such type of behaviour (i.e., temperature dependent) of conductivity is observed in the similar compound, such as $\text{Bi}(\text{Zn}_{2/3}\text{Nb}_{1/3})\text{O}_3$ [29].

Figure 10 illustrates the temperature dependence of dc conductivity ($\log \sigma_{dc}$) as a function of reciprocal of temperature. From the plot, it can be seen that the rise in conductivity of the material is nearly linear with increase of temperature indicating negative temperature coefficient of resistance (NTCR) behaviour of the compound. As the dc conductivity is also a thermally activated process, the nature of the above plot again follows the Arrhenius

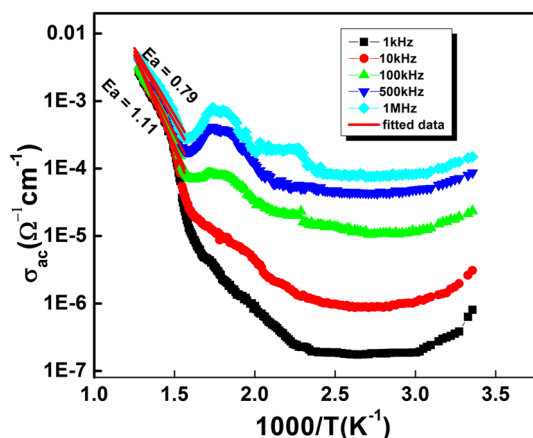


Fig. 9 Temperature dependent ac conductivity at selected frequency of $\text{Bi}(\text{Zn}_{2/3}\text{Ta}_{1/3})\text{O}_3$.

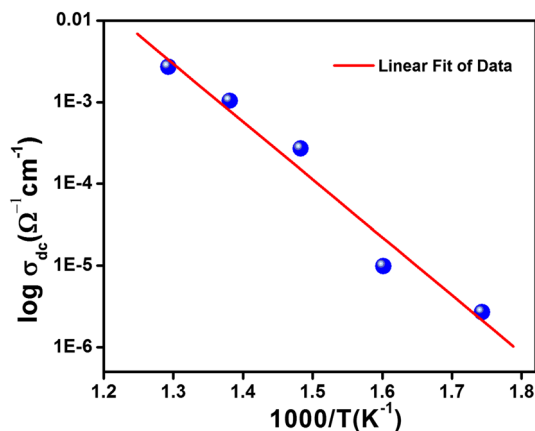


Fig. 10 Dc conductivity as a function of inverse of absolute temperature of $\text{Bi}(\text{Zn}_{2/3}\text{Ta}_{1/3})\text{O}_3$

relation: $\sigma_{\text{dc}} = \sigma_0 \exp(-E_a/kT)$, where the terms have usual meanings [30].

Under the effect of temperature and frequency, complex modulus spectrum of materials is a very valuable tool to identify electrical conductivity mechanism, interfacial effect, bulk properties, grain-boundary conduction effects and electrode polarization. The imminent characteristics of relaxation mechanism and electrical processes occurring in the polycrystalline compound can also be explored significantly using this technique [31, 32]. Figure 11 presents the variation of both the components (M' vs M'') of electric modulus at different temperatures (100–500 °C) of $\text{Bi}(\text{Zn}_{2/3}\text{Ta}_{1/3})\text{O}_3$. In the M' versus frequency plots, it can be seen that with the increase in temperature, the finite value of M' approaches to zero on lowering the frequency, while the entire M' spectra have a tendency to overlap one another at high-frequency and high-temperature due

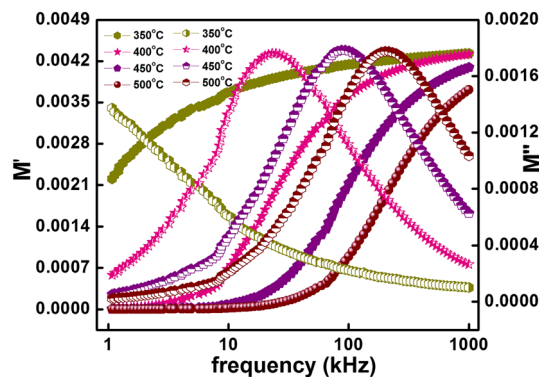


Fig. 11 Frequency variation of real and imaginary part of electric modulus at some high-temperatures of $\text{Bi}(\text{Zn}_{2/3}\text{Ta}_{1/3})\text{O}_3$

to the occurrence of conduction phenomenon and mobility of shorter range charge carriers which signifies that for movement of charges a lack of restoring force is caused by the effect of steady electric field. It can be noticed in the figure (M'' versus frequency) that the M''_{max} relaxation peak advances to the higher frequency region with the enhancement in temperature which implies that the dielectric relaxation rate rises with increase in temperature. This movement of dielectric relaxation peak indicates that mostly at higher-temperatures, the hopping mechanism of charge carriers dominates in thermally activated process. Furthermore, the existence of non-Debye type relaxation behaviour is illustrated from the unsymmetrical peak broadening which suggests the spread of relaxation time with different time constants.

4 Conclusion

$\text{Bi}(\text{Zn}_{2/3}\text{Ta}_{1/3})\text{O}_3$ compound has been synthesized by a standard high-temperature mixed oxide technique. Study of basic crystal structure of the prepared material at room temperature using X-ray diffraction pattern exhibits the formation of phase-pure orthorhombic crystal system. It is found that replacement of niobium of $\text{Bi}(\text{Zn}_{2/3}\text{Nb}_{1/3})\text{O}_3$ by tantalum has significantly modified the structural, micrographs, dielectric, impedance, modulus, conductivity characteristics have been modified by addition of tan. Analysis of impedance of the sample reveals the existence of semiconducting characteristics (concluded from negative temperature coefficient of resistance) as well as occurrence of grain and bulk boundary effects in the material. Using impedance spectroscopy technique, the parameters of transport properties (electrical conductivity) of BZT have been estimated. The dielectric relaxation in the sample has been studied from the extracted by modulus analysis which implies that in the synthesized sample conductivity relaxation is of non-Debye type. The

structure–property relationship and electrical phenomena happening inside the material have been demonstrated by the proposed equivalent circuit model. Based on the physical parameters and characteristics, the fabricated non-lead perovskite (BZT) compound can be considered as a good candidate for some applications.

References

1. S.M. Zanettia, S.A. Silvab, *Mater. Res.* **10**, 261 (2007)
2. M. Valant, P.K. Davies, *J. Mat. Sci* **34**, 5437 (1999)
3. I. Levin, T.G. Amos, J.C. Nino, *J. Solid State Chem.* **168**, 69 (2002)
4. S. Bhuyan, J. Hu, C.Q. Sun, *J. Appl. Phys.* **103**, 094915 (2008)
5. A.K. Tagantsev, J.W. Lu, S. Stemmer, *Appl. Phys. Lett.* **86**, 032901 (2005)
6. S. Singh, A.K. Mondal, S.B. Krupanidhi, *Adv. Sci. Lett.* **2**, 356 (2009)
7. M.T. Sebastian, (Elsevier Ltd., Amsterdam, 2008)
8. D. Zhou, W.B. Li, L.Pang, J. Guo, Z.M. Qi, T. .Shao, C.A. Randali, *RAC Adv.* **43**, 7290 (2014)
9. S.N. Das, S.K. Pradhan, S. Bhuyan, R.N.P. Choudhary, *J. Mater. Sci. Mater. Electron.* (2017). <https://doi.org/10.1007/s10854-017-7845-y>
10. L.E. Cross, *Relaxor Ferroelectr. Ferroelectr.* **76**, 24 (1987)
11. S.N. Das, S. Pradhan, S. Bhuyan, R.N.P. Choudhary, P. Das, *J. Electron. Mater.* **46**, 1637 (2017)
12. G.A. Samara, *J. Phys. Condens. Matter.* **15**, 367 (2003)
13. C.V. Madhusudhana, R.G. Prasad, *Bull. Mater. Sci.* **35**, 579 (2012)
14. S. Bhuyan, K. Sivanand, S.K. Panda, R. Kumar, J. Hu, *IEEE Magn. Lett.* **2**, 6000204 (2011)
15. C.H. Weng, W.C.J. Wei, *J. Am. Ceram. Soc.* **93**, 3124 (2010)
16. P.K. Bajpai, K.N. Singh, *Indian J. Mater. Sci.* **2013**, 7 (2013). <https://doi.org/10.1155/2013/927908>
17. I.N. Lin, C.T. Chia, H.L. Liu, H.F. Cheng, R. Freer, *J. Appl. Phys.* **102**, 044112 (2007)
18. H.P. Klug, L.E. Alexander, *X-ray Diffraction Procedures for Polycrystalline and Amorphous Materials* (Wiley-Interscience, New York, 1974)
19. B.D. Cullity, *Elements of X-ray Diffraction* (Addison-Wesley, Reading, 1978)
20. https://en.wikipedia.org/wiki/Goldschmidt_tolerance_factor. Accessed 20 Oct 2017
21. B.N. Parida, P.R. Das, R. Padhee, R.N.P. Choudhary, *J. Mater. Sci. Mater. Electron.* **27**, 342 (2016)
22. S.K. Pradhan, S.N. Das, S. Bhuyan, C. Behera, R. Padhee, R.N.P. Choudhary, *Appl. Phys. A* **122**, 604 (2016)
23. K.K. Mishra, A.T. Satya, A. Bharathi, V. Sivasubramanian, V.R.K. Murthy, A.K. Arora, *J. Appl. Phys.* **10**, 123529 (2011)
24. S.N. Das, A. Pattanaik, S. Kadambini, S. Pradhan, S. Bhuyan, *J. Mater. Sci. Mater. Electron.* **27**, 10099 (2016)
25. Y. Liu, J. Wei, Y. Liu, X. Bai, P. Shi, S. Mao, X. Zhang, C. Li, B. Dkhil, *J. Mater. Sci. Mater. Electron* **27**, 3095 (2016)
26. V. Provenzano, L.P. Boesch, V. Volterra, C.T. Moynihan, P.B. Macedo, *J. Am. Ceram. Soc.* **55**, 492 (1972)
27. H. Jain, C.H. Hsieh, *J. Solids Non Cryst.* **172**, 1408 (1994)
28. D.P. Almond, A.R. West, *Solid State Ion.* **11**, 57 (1983)
29. S. Halder, K. Parida, S.N. Das, S. Bhuyan, R.N.P. Choudhary, *J. Mater. Sci. Mater. Electron.* **28**, 15928 (2017)
30. R. Jacob, H.G. Nair, J. Isac, *Process. Appl. Ceram.* **9**, 73 (2015)
31. J. Liu, C.G. Duan, W.G. Yin, W.N. Mei, R.W. Smith, J.R. Hardy, *J. Chem. Phys.* **119**, 2812 (2003)
32. R. Macdonald, *Solid State Ion.* **13**, 147 (1984)